Influence of base course thickness on the deformation behavior of geogrid-reinforced pavement

Aung Aung Soe, Jiro Kuwano, Ilyas Akram & Takaya Kogure
Saitama University, Japan

ABSTRACT: Deformation behavior of model pavement section was investigated through large-scale laboratory tests. Six cyclic loading tests were performed with base course thicknesses of 3 cm, 5 cm and 10 cm for no reinforcement and geogrid reinforcement respectively. Cyclic pressure with varying magnitudes was applied in each test, ranging from 50 kPa to 400 kPa allowing 500 cycles for each pressure level. Test results revealed that the influence of base course thickness was more obvious on the unreinforced sections than the geogrid-reinforced ones in which this influence was noticed on the subgrade settlement behavior. Regardless of reinforcement condition, surface settlement was mainly attributed to the subgrade settlement of the thin sections, while both subgrade settlement and lateral flow resulted in the surface settlement of the thick sections. The effect of base course thickness was minimal on the rebound characteristics, which was proportional to the applied pressure level. The accumulative loss of base course thickness was significant in the thick sections and increased with increasing pressure. This loss was effectively reduced by including the geogrid reinforcement. However, this reduction was started notice under 150 kPa. Compared to the unreinforced tests, the potential benefits of geogrid stabilization were known by means of reductions in the settlement and the loss of base course thickness.

Keywords: base course thickness, pavement, geogrid, cyclic loading, deformation

1 INTRODUCTION

Since geosynthetic materials have been developed, they were used in many geotechnical applications such as reinforced soil walls, embankments and so forth. Depending on the type of applications and purposes, there are several types of geosynthetic materials, like geotextile, geocell, geogrid and so on. For the flexible pavement, geogrid has been mainly used to reinforce and/or stabilize the structural layers, which are (1) asphalt concrete layer, (2) base course layer, (3) subbase layer, and (4) subgrade layer (Zornberg, 2012). Based on the design traffic volume and requirements, flexible pavement can be the paved or unpaved condition. Generally, the strength of the existing soil, so called subgrade, is not enough to support the wheel load. Thus, the aggregate materials are used as base course layer above the subgrade layer. This material must have sufficient strength to support the load without lateral shear and must have sufficient thickness to distribute the vertical load over a wider area of subgrade layer (Giroud & Han, 2004).

In general, longitudinal depression along the wheel path, so called rutting, is the primary distress mechanism during accelerated pavement testing (Kazmee & Tutumluer, 2015). According to Dawson and Kolisoja (2006), this rutting in flexible pavement can occur due to the combination of different modes. They are (1) mode 0, which is due to the compaction of non-saturated materials in the pavements, (2) mode 1, which is due to the inadequate shear strength in the aggregate relatively close to the pavement surface, (3) mode 2, which is due to the shear deformation within the subgrade layer, and (4) mode 3, which is due to the particle damage.

With the development and application of geosynthetics in flexible pavement, the potential improvements have been known and described as traffic benefit ratio (TBR) and base course reduction (BCR) (Zornberg,

2012). However, it is still needed to understand the reinforcement mechanisms of geosynthetic reinforcement. These mechanisms can be different depending on the geosynthetic types. For geogrid, the lateral restraint effect or confinement can be regarded as the primary reinforcement mechanism (Anderson, 2006). Since there are various types of geogrid such as uniaxial, biaxial and multiaxial geogrids, this confinement effect may also be varied with their properties and aggregate used. In this study, the recently developed multiaxial geogrid was used and its reinforcement behavior was examined by conducting laboratory experiments. The deformation behavior of the geogrid-reinforced aggregate layer was mainly investigated by considering aggregate thickness and different pressure levels. In this study, the potential mode of deformation will be investigated for the geogrid-reinforced base course layer.

2 EXPERIMENTAL PROGRAM

In this study, six cyclic loading tests were performed, including three unreinforced tests and three geogrid-reinforced tests. Tests were modelled in the laboratory, considering the base course thicknesses as 3 cm, 5 cm and 10 cm. In all reinforced cases, geogrid was placed at the bottom of base course layer. In each test, cyclic load was applied with varying pressures, ranging from 50 kPa to 400 kPa. Each pressure level was allowed for 500 load cycles. For the failure criterion, AASHTO (1993) stated that the typical allowable rut depths range from 25.4 mm to 50.8 mm (1.0 to 2.0 inches). The failure criterion was taken as 45 mm in the current study.

3 MATERIALS

3.1 *Model subgrade and base course*

The subgrade layer and base course layer were modelled by using fine silica sand and coarse silica sand. The fine silica sand has the following index properties: soil particle density ρ_s = 2.675 g/cm^3, uniformity coefficient C_u = 1.98, curvature coefficient C_c = 0.943, mean diameter D_{50} = 0.488 mm, maximum dry density $\rho_{d,max}$ = 1.628 g/cm^3, and minimum dry density $\rho_{d,min}$ = 1.338 g/cm^3. For coarse silica sand, the properties are: C_u = 1.904, C_c = 0.879, and D_{50} = 3.735 mm. This coarse sand was selected because it is the largest coarse sand, commercially available in Japan, and its average particle size is greater than the rib thickness and junction thickness of the geogrid used. Since C_u and C_c of both sands are not in the range, $C_u > 6$ and $1 < C_c < 3$, specified by the Unified Soil Classification System (USCS), both sands can be regarded as poorly graded sands (SP). The particle size distribution curves of the model subgrade and base course materials are shown in Figure 1.

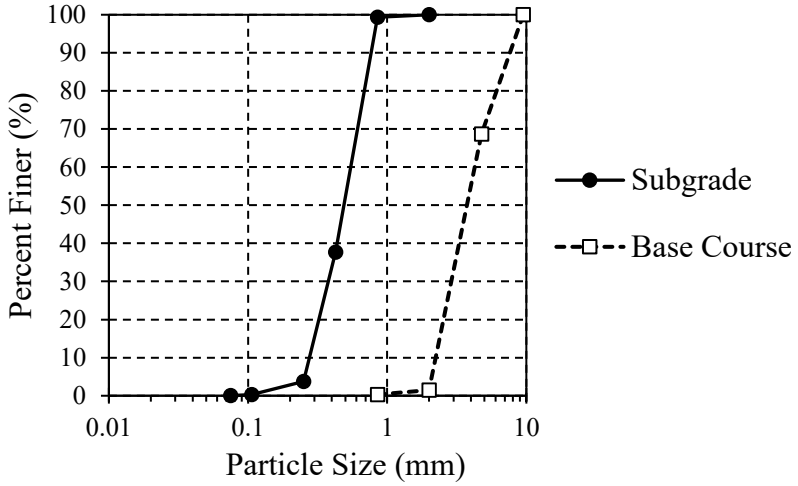

Figure 1. Particle size distribution curves of model subgrade and base course materials

3.2 *Geogrid for reinforcement*

The multiaxial geogrid with triangular aperture was used for the reinforcement in this study. This geogrid has been recently developed by Tensar. According to manufacturer, this geogrid has the tensile strength of

10 kN/m in the cross-machine direction and diagonal directions, pitch length of 40 mm along each side of triangular aperture, and unit weight of 245 g/m^2.

4 EEXPERIMENTAL SETUP AND TESTING PROCEDURE

In this experimental study, a large square container (100 cm x 100 cm x 80 cm) was used for the preparation of model pavement sections. Side walls of the container are firmly supported by the rigid steel frames. A rigid circular steel plate, diameter = 17.5 cm, was used for the model trafficked load simulation. This plate size was selected so that the size ratio of container and plate was large enough (100/17.5 ≈ 6.0) to minimize the boundary interference (Alawaji, 2001; Yetimoglu et al., 1994). In each test, the total depth of the model soil layers was prepared to be greater than 70 cm depth. For this depth, the boundary influence would be minimal according to Boussinesq Stress Distribution Analysis.

In order to model the subgrade layer, sand raining method was adopted and applied in accordance with the previous studies (Dave & Dasaka, 2012; Miura & Toki, 1982; Vaid & Negussey, 1984). By using this method, the relatively high densities of subgrade layer were achieved, ranging from 1.58 g/cm^3 to 1.61 g/cm^3. When the subgrade layer reached the desired thickness, it was levelled by using the soft brush, in order not to disturb the soil density. Then, a small plastic plate was placed at the predetermined point, which was directly below the footing. A small aluminum tube was set above the small plate. Subgrade settlement was monitored via this tube, during the test. For the model base course preparation, coarse sand was uniformly distributed over the subgrade layer, followed by manual compaction. For each lift, 80 kg of coarse sand was used and compacted to achieve the average thickness of 5 cm, except 3 cm thick tests in which 48 kg mass was used. In each test, the density of base course layer was controlled to be 1.60 g/cm^3 in average.

After the preparation of subgrade and base course layers, the model footing was placed at the predefined location, so that the aluminum tube could pass through the footing. A linear variable displacement transducer was set on the footing to measure the surface settlement, while another transducer was used to monitor the subgrade settlement. Before cyclic pressure was applied, a seating pressure of 10 kPa was applied to the footing. To simulate the variable magnitudes of trafficked loading, the cyclic trapezoidal load-pulse was applied with a frequency of 0.1 Hz and the load magnitude was varied from 50 kPa to 400 kPa. Each loading step was allowed for 500 load cycles until the footing settlement reached over 45 mm. In each test, data were recorded by a data acquisition system at every 1 second. The schematic layout of the test setup is shown in Figure 2.

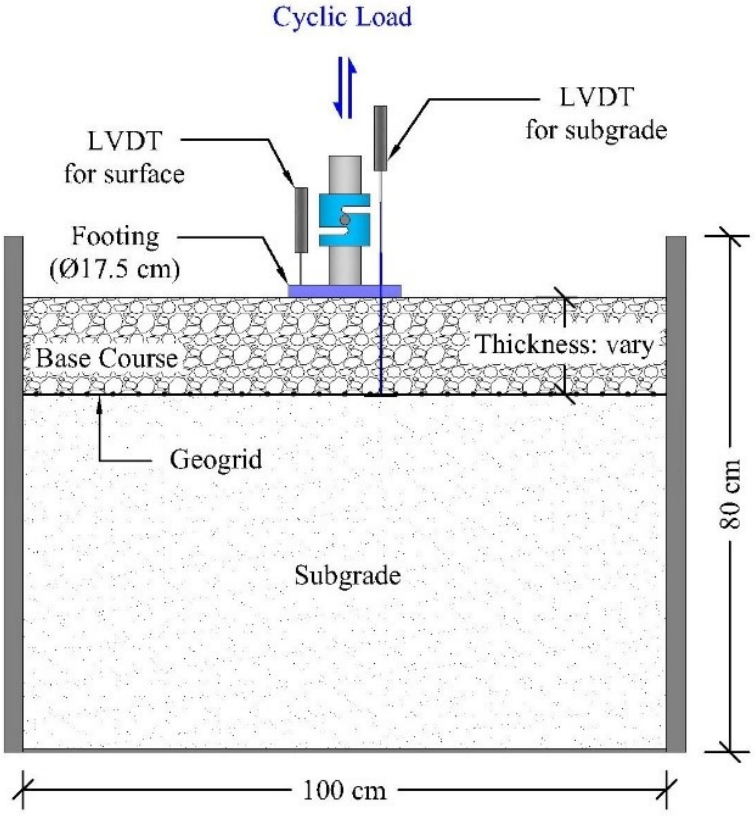

Figure 2. Schematic layout of test setup

5 RESULTS AND DISCUSSION

5.1 *Influence of base course thickness on the surface and subgrade settlements of unreinforced layer*

Three unreinforced tests were performed with the base course thicknesses: 3 cm, 5 cm and 10 cm. From each test, the permanent deformations of surface and subgrade layers were taken when the footing pressure was minimum in each load cycle. The variations of these permanent deformations are presented in Figure 3, against load cycles and footing pressures.

As seen in Figure 3a, the permanent surface settlements were almost same under 50 kPa pressure. For 10 cm thick section, the improvement was started notice under 100 kPa, while it was observed under 150 kPa for 5 cm thick section. These improvements were more significant with the increase in pressure and load cycles. This was because the layer modulus of base course might increase with increasing thickness, resulting in smaller deformation.

For the 3 cm thick base course, the permanent surface deformation increased rapidly with increasing load cycles under 150 kPa and 200 kPa. This surface deformation was contributed by the underlaying subgrade layer. As shown in Figure 3b, the surface and subgrade settlements of 3 cm thick section are similar under the given pressure level. The progressive increment of subgrade settlement implied that the stress concentration on subgrade under 200 kPa would have been larger than the bearing strength of subgrade layer. Under 300 kPa, this section failed suddenly within a few load cycles.

For 5 cm and 10 cm thick sections, failures were also observed under 300 kPa pressure. 10 cm thick section withstood nearly 500 cycles, while 5 cm section failed within 50 load cycles. Although surface settlement of 10 cm section predominantly increased during initial loading of 300 kPa, the rate increment in settlement slightly declined with load cycles. Unlike 3 cm thick base course, the behavior of surface and subgrade settlements were different for 5 cm and 10 cm thick sections, as presented in Figure 3. Due to their larger thicknesses, the stress concentration on subgrade might be less in these sections, compared to 3 cm section. However, the sudden increase in subgrade settlements were noticed in 5 cm and 10 cm thick sections under the initial load cycles of 300 kPa. This was because the driving shear stresses under 300 kPa might cause the lateral shear flow within the base course layer. As a result, the effective thickness of base course decreased as soon as this lateral shear flow occurred. Hence, the stress concentration suddenly increased on subgrade layer, resulting in the rapid increase in the subgrade settlement.

For 10 cm thick section, the increasing trend of subgrade settlement became slower with load cycles. This means that a stable condition was again achieved in this section after lateral flow had occurred. Due to lateral flow, the obvious surface bulging was noticed near the circumference of footing. This bulging would add some overburden stresses on the subgrade layer, and, hence, the bearing strength of subgrade might increase in some amount. Therefore, a slight declination was observed with increasing load cycle. From these results, it was known that the surface settlement was mainly contributed by subgrade settlement in thin layer, and by both subgrade settlement and lateral shear flow in thick base course layer.

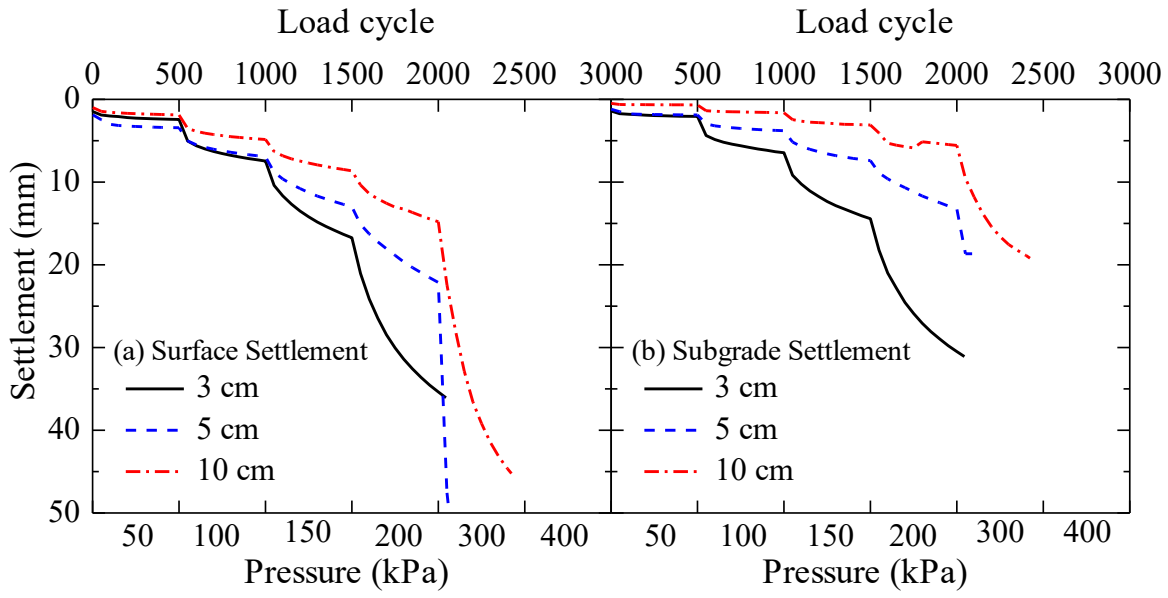

Figure 3. Permanent settlements of surface and subgrade for unreinforced layer

5.2 *Influence of base course thickness on surface and subgrade settlements of geogrid-reinforced layer*

Three tests were carried out with geogrid reinforcement at the bottom of the base course layer. The recorded permanent settlements of surface and subgrade are presented in Figure 4. As seen in Figure 4a, unlike in the unreinforced tests, the differences among the permanent surface settlements were not so obvious until the end of 200 kPa pressure. Under 300 kPa, the rates of surface settlement in all cases abruptly increased with load cycles, which was more significant in 3 cm thick section. These rates increased more rapidly under 400 kPa. Despite having the thicker layer, the surface settlement of 10 cm section failed after 200 load cycles of 400 kPa, same as that of 3 cm section. On the other hand, 5 cm thick section withstood until almost 500 cycles. This behavior can be explained from the subgrade deformation behavior, as shown in Figure 4b. The subgrade settlement of 3 cm section was almost same in magnitude as the surface settlement. This implied the surface settlement of 3 cm section was mainly contributed by the subgrade layer deformation, which was similar in behavior of 3 cm thick unreinforced test. However, the subgrade settlement of 10 cm section was different in manner from its surface settlement. This means that the lateral shear flow in 10 cm thick base course layer contributed the surface settlement, in addition to the subgrade settlement. The similar characteristics was also observed in the unreinforced 10 cm thick test.

For 5 cm thick section, the subgrade settlement was slightly less than the surface settlement under the respective pressure conditions. This implied the lateral shear flow inside base course layer might be smaller than that in 10 cm case. Because of the smaller thickness, geogrid reinforcement could contribute the effective confinement to the whole 5 cm thickness. Hence, the layer became stiffer and showed the slower rate of increase in surface settlement. As seen in Figure 4b, the subgrade settlement became smaller with the increase in the base course thickness. This behavior was also known in the unreinforced tests, however, the settlements were significantly small in all geogrid-reinforced tests. In geogrid-reinforced tests, the applied stresses at the subgrade layer were reduced by the geogrid (Sun et al., 2015), which can distribute the stresses to the wider area, resulting in the smaller settlement of subgrade layer. The test results showed the effect of base course thickness was minimal on the surface settlement of geogrid-reinforced sections, while its influence was obvious on subgrade settlement. This was because geogrid could not fully confine the whole thickness when the base course became thicker, in which the surface settlement was mainly attributed to the lateral flow of materials. However, the thicker the base course was, the smaller the stress concentration on subgrade layer, resulting in smaller settlement of subgrade layer.

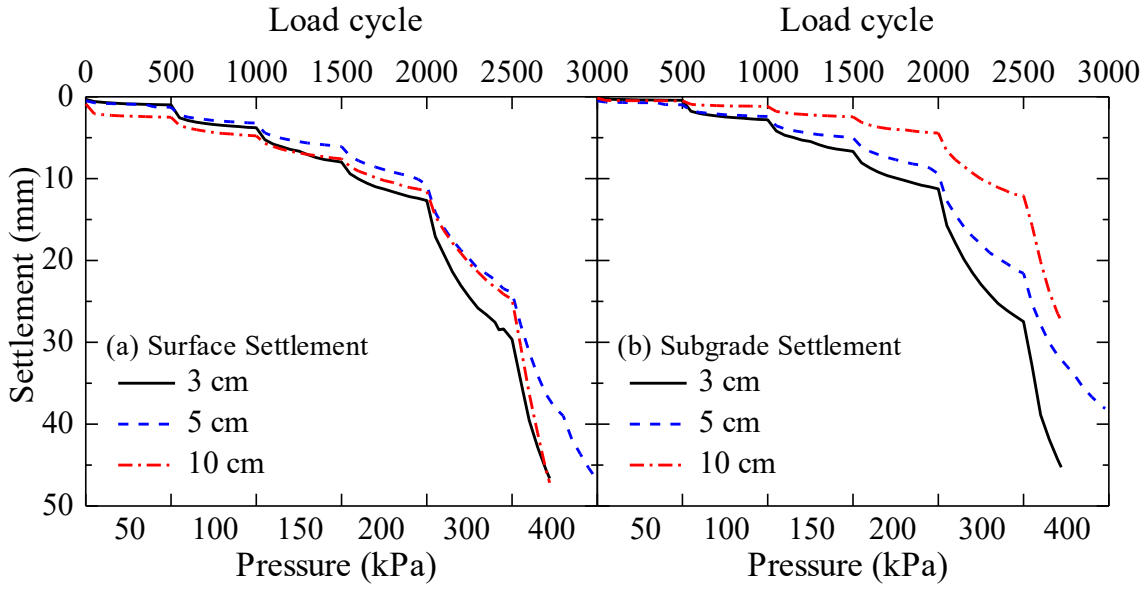

Figure 4. Permanent settlements of surface and subgrade for geogrid-reinforced layer

5.3 *Rebound deformation behavior of surface and subgrade layers*

The behavior of rebound deformation was examined for the unreinforced tests and the geogrid-reinforced tests. In order to know the benefit of geosynthetic reinforcement in a mechanistic-empirical pavement design method, the resilient modulus and permanent deformation behavior must be considered (Yang & Han, 2013). This resilient modulus is used to calculate the rebound of a pavement after the loading by a truck tire (Briaud J. L., 2001). In this study, the rebound deformation was calculated, based on the settlements at

maximum and minimum footing pressures in each cycle. This rebound deformation behavior was analyzed between the unreinforced case and the geogrid-reinforced case in this study, instead of using resilient modulus. The variations of the average rebound deformation (for 50 cycles) of surface and subgrade layers are presented in Figure 5, together with load cycles under each pressure level.

In Figure 5, the rebound deformations were presented for the respective base course thicknesses, denoted with prefixes "N" for no reinforcement and "G" for geogrid reinforcement. As seen in Figure 5a, the surface rebound deformations were similar to each other, regardless of reinforcement condition and base course thickness, until the end of 200 kPa. These deformations increased with increasing pressure and became stable within a few load cycles. However, under 300 kPa, the increasing trends with load cycles were noticed in G-3 cm and G-5 cm tests, while a decreasing trend was found in G-10 cm test. This was because the tension membrane effect of geogrid reinforcement might have been occurred in these thin sections (3 cm and 5 cm) under 300 kPa pressure. With this bending action, the geogrid would recover to its original shape during unloading stage. As a result, the increasing tendencies of the surface rebound were observed in these sections. It can be assumed that geogrid bending deformation might have been in the elastic state under 300 kPa pressure. However, under 400 kPa, the sudden drops in rebounds were observed in both sections, because they had already failed by punching manner and geogrid might not be able to recover its original shape under the progressive punching deformation.

For 10 cm thick sections (N-10 cm & G-10 cm, of which lines are overlapping), the surface rebounds decreased with increasing load cycles under 300 kPa. Under this pressure, the driving shear stresses would be larger than the frictional shear strength of aggregate materials. Due to lateral flow of materials under loading, these 10 cm thick sections could not rebound to the large amount under unloading, as compared to the thin sections. In thin sections, geogrid could be able to confine the whole thickness of base course layer. Hence, these layers became stiffer, resulting in the larger rebound deformations. Under 400 kPa, G-10 cm test showed an increasing trend with load cycles. Since the base course thickness had already been reduced under the previous loading stage, geogrid would confine this reduced thickness again. Therefore, the rebound deformation became larger with load cycle under 400 kPa. Unlike the thin sections, the sudden drop in rebound was not observed in G-10 cm test because the geogrid might recover to its shape under the unloading state of 400 kPa.

Compared to the surface rebound, the rebound of subgrade layer was large under the respective pressures, as shown in Figure 5b. Because of the overburden effect from base course and lower stress level at subgrade, the elastic rebound of subgrade was greater than that of surface rebound under unloading. Unlike surface rebound, the effect of geogrid was observed under 200 kPa and following pressures. The subgrade rebound of geogrid-reinforced sections, regardless of thickness, showed the larger values than that of unreinforced section (N-10 cm). This was obvious with the increase in pressure. Sun et al. (2015) also reported that the resilient deformations in the stabilized sections increased significantly under a higher load magnitude and were larger than those of the un-stabilized sections. However, the effect of geogrid reinforcement was not observed on the behavior of surface rebound deformation in this study. This might be due to low shear resistance of base course materials used in this study. Because of this, the aggregate materials might not be able to recover to their original positions under the unloading state. Hence, the similar characteristics of the surface rebound were observed between the unreinforced tests and the geogrid-reinforced tests.

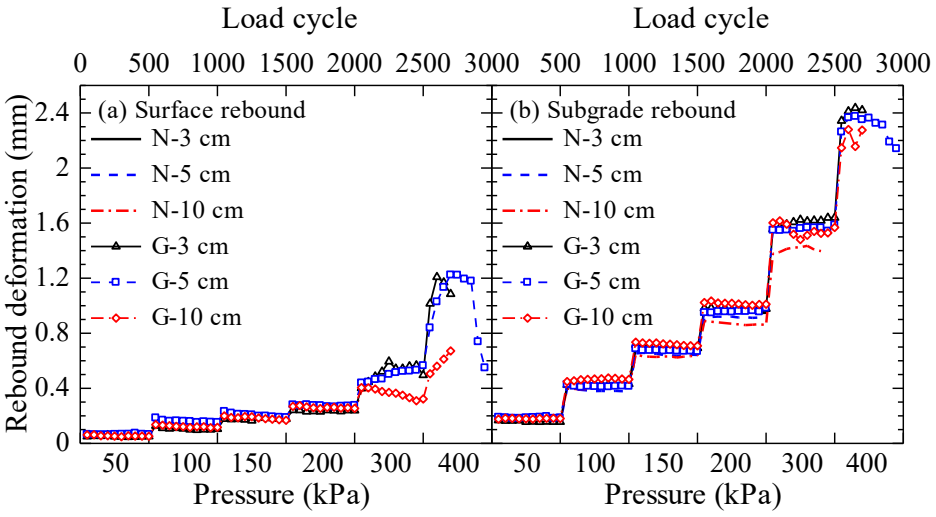

Figure 5. Rebound deformation behavior of unreinforced (N) and geogrid-reinforced (G) layers

5.4 *Accumulative loss of base course layer thickness (h_l)*

In order to know the change in thickness, the accumulative loss of base course layer (h_l) was calculated, considering the surface settlement (S_f) and the subgrade settlement (S_s). The accumulative loss, h_l, is the summation of the rate differences between surface settlement and subgrade settlement in each load cycle under the given pressure level. This calculation is simply formulated and presented in equation (1).

$$h_l = \sum (\Delta S_f - \Delta S_s) \tag{1}$$

where h_l = accumulated loss in base course layer thickness, ΔS_f = rate of surface settlement in each load cycle, ΔS_s = rate of subgrade settlement in each load cycle. Under each pressure level, the rate differences were summed up for 500 load cycles and this sum was added to the value obtained in the previous loading level. In this way, the incremental loss of base course layer thickness was calculated. The incremental loss in thickness for each test is presented in Figure 6, against pressure.

As seen in Figure 6, the accumulative loss of base course layer thickness, h_l, increased proportionately with increasing pressure. This loss was significantly large in the thick unreinforced sections, N-5 cm and N-10 cm, and the thick reinforced section, G-10 cm. For the unreinforced sections, the accumulative loss values dramatically increased and reached almost 9 mm when these sections failed under 300 kPa pressure level, as shown in Figure 3. In these sections, the shear stresses would cause the lateral flow of base course materials due to the poor frictional resistance. For N-3 cm test, the values were smaller than those of other unreinforced tests under the respective pressure levels. In this test section, the surface settlement was mainly attributed to the underlaying subgrade settlement, rather than the lateral flow. Hence, the smaller losses in base course were observed in N-3 cm section. For N-5 cm and N-10 cm tests, the accumulative values were almost same under the given pressure level. This implied that there must be the constant trend of the accumulative loss for this particular type of base course material. This was because the thickness of base course had the negligible influence on the h_l values after a certain thickness. For the given aggregate type, this thickness may exist between 3 cm and 5 cm. However, this may vary with the aggregate type used.

For the geogrid-reinforced tests, the reductions in h_l values were noticed under 150 kPa and afterwards, compared to the unreinforced tests. These reductions were more pronounced with the increase in pressure for the respective thicknesses. Until the end of 100 kPa, the differences between the unreinforced case and the geogrid-reinforced case were not significant, because the aggregate materials might have been densified and driven to strike through the geogrid aperture. As soon as the interlocking between geogrid and aggregate particles was achieved, this would initiate the confinement action of geogrid and, hence, the reductions in h_l value were observed. Unlike the unreinforced cases (N-5 cm and N-10 cm), h_l values of G-5 cm and G-10 cm tests were obviously different. The trend of increasing h_l in G-5 cm test was flatter than that of G-10 cm test and was parallel to that of G-3 cm test with a certain offset. This implied that the effective confinements were achieved in 3 cm and 5 cm thick sections by the inclusion of geogrid. However, geogrid might not be able to confine the whole 10 cm thickness, resulting in the greater loss of thickness. From these test results, it was realized that the loss of base course thickness could be reduced by the inclusion geogrid reinforcement. This reduction was more obvious in the thinner sections.

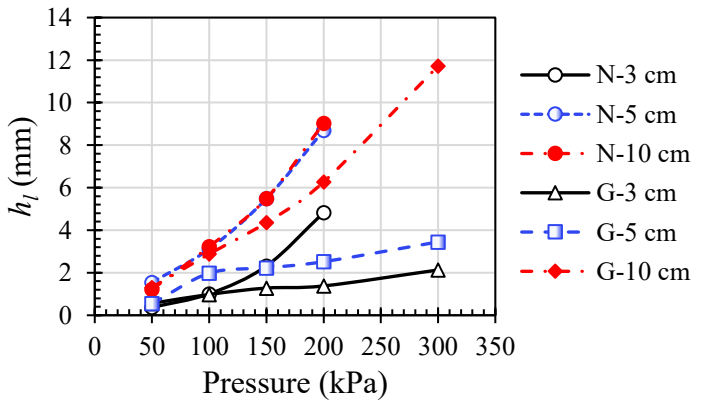

Figure 6. Accumulative loss of base course layer thickness

6 CONCLUSIONS

Laboratory model tests were performed to investigate the effect of base course thickness on the deformation behavior of geogrid-reinforced pavement. Six cyclic loading tests were carried out, considering three different base course thicknesses for no reinforcement and geogrid reinforcement respectively. Test results revealed that the influence base course thickness was more pronounced on the unreinforced sections than geogrid-reinforced sections, for which this influence was observed on the subgrade layer settlement. Regardless of reinforcement condition, the surface settlement was mainly contributed by the subgrade layer settlement in thin base course sections. On the other hand, this surface settlement was attributed to the lateral flow of aggregate materials and the subgrade layer settlement in the thick sections. Regarding the rebound characteristic, the effect of geogrid reinforcement was noticed only in the subgrade under 200 kPa and afterwards. This rebound deformation is proportional to the applied pressure level. From the settlements of surface and subgrade, the accumulative loss of base course thickness was calculated for each test. Under the given pressure, this loss is more significant in the thicker sections in which lateral flow of aggregate materials dominated. This loss of base course thickness was effectively reduced by means of geogrid reinforcement. The reduction was started noticed under 150 kPa loading stage in all reinforced tests and it was more obvious in the thin section in which geogrid would fully confine the whole thickness. Compared to the unreinforced tests, the benefits of geogrid reinforcement were known in the reduction of the settlement and in the reduction of the base course thickness loss due to lateral flow of materials.

ACKNOWLEDGEMENTS

This study was collaborated with NIPPO CORPORATION and MITSUI CHEMICALS INDUSTRIAL PRODUCTS LTD. Their continuous supports are highly appreciated.

REFERENCES

AASHTO. (1993). *Guide for Design of Pavement Structures*. Washington, D.C., USA.

Alawaji, H. A. (2001). Settlement and bearing capacity of geogrid-reinforced sand over collapsible soil. *Geotextiles and Geomembranes*, *19*(2), 75–88. http://doi.org/10.1016/S0266-1144(01)00002-4

Anderson, R. P. (2006). Geogrid Separation. *Proceedings of International Conference on New Developments in Geoenvironmental and Geotechnical Engineering*. Incheon, Republic of Korea.

Briaud, J. L. (2001). Introduction to Soil Moduli. *Geotechnical News*. BiTech Publishers Ltd. Richmond, B.C., Canada.

Dave, T. N., & Dasaka, S. M. (2012). Assessment of portable traveling pluviator to prepare reconstituted sand specimens. *Geomechanics and Engineering*, *4*(2), 79–90. http://doi.org/10.12989/gae.2012.4.2.079

Dawson, A., & Kolisoja, P. (2006). *Managing Rutting in Low Volume Roads: Executive Summary of Roadex III Project*. Northern Periphery, EU. http://www.roadex.org/services/knowledge-center/publications/permanent-deformation/

Giroud, J. P., & Han, J. (2004). Design method for geogrid-reinforced unpaved roads . I . development of design method. *Journal of Geotechnical and Geoenvironmental Engineering*, *130*(8), 775–786.

Kazmee, H., & Tutumluer, E. (2015). *Evaluation of aggregate subgrade materials used as pavement subgrade/granular subbase*. Research report FHWA-ICT-15-013, Illinois Center for Transportation.

Miura, S., & Toki, S. (1982). A Sample preparation method and its effect on static and cyclic deformation-strength properties of sand. *Soils and Foundations*, *22*(1), 61–77. http://doi.org/10.3208/sandf1972.22.61

Sun, X., Han, J., Kwon, J., Parsons, R. L., & Wayne, M. H. (2015). Radial stresses and resilient deformations of geogrid-stabilized unpaved roads under cyclic plate loading tests. *Geotextiles and Geomembranes*, *43*(5), 440–449. http://doi.org/10.1016/j.geotexmem.2015.04.018

Vaid, Y. P., & Negussey, D. (1984). Relative density of pluviated sand samples. *Soils and Foundations*, *24*(2), 101–105. http://doi.org/10.1248/cpb.37.3229

Yang, X., & Han, J. (2013). Analytical model for resilient modulus and permanent deformation of geosynthetic-reinforced unbound granular material. *Journal of Geotechnical and Geoenvironmental Engineering*, *139*(9), 1443–1453. http://doi.org/10.1061/(ASCE)GT.1943-5606.0000879

Yetimoglu, T., Wu, J. T. H., & Saglamer, A. (1994). Bearing capacity of rectangular footings on geogrid-reinforced sand. *Journal of Geotechnical Engineering*, *120*(12), 2083–2099.

Zornberg, J. G. (2012). Geosynthetic-reinforced pavement systems. *5th European Geosynthetics Congress:* Proceedings keynote lectures & educational session, 49–61. Valencia.